Monthly Notices
of the
ROYAL ASTRONOMICAL SOCIETY

MNRAS **471,** 4910–4916 (2017)
Advance Access publication 2017 August 2

doi:10.1093/mnras/stx1938

A model for a photoionized, conical jet from a young, massive star

A. C. Raga,[1⋆] J. Cantó,[2] A. Tinoco-Arenas,[3] J. C. Rodríguez-Ramírez,[1] L. F. Rodríguez[4⋆] and S. Lizano[4⋆]

[1]*Instituto de Ciencias Nucleares, Universidad Nacional Autónoma de México, Ap. 70-543, 04510 Cd. Mx., Mexico*
[2]*Instituto de Astronomía, Universidad Nacional Autónoma de México, Ap. 70-468, 04510 Cd. Mx., Mexico*
[3]*Instituto de Geofísica, Universidad Nacional Autónoma de México, 04510 Cd. Mx., Mexico*
[4]*Instituto de Radioastronomía y Astrofísica, Universidad Nacional Autónoma de México, A.P. 3-72 (Xangari), 58089 Morelia, Michoacán, Mexico*

Accepted 2017 July 26. Received 2017 July 25; in original form 2017 June 29

ABSTRACT

We consider a conical jet from a massive, young star, which also powers a compact H II region. The high density at the base of the jet traps the stellar, ionizing radiation, so that the jet beam is neutral (at larger distances). This neutral beam then becomes progressively photoionized by the diffuse, ionizing radiation field emitted by the surrounding H II region. We derive a simple, analytic model for this flow, and use it to calculate the contrast between the free–free emission of the jet and the background H II region. We find that for appropriate parameters, the jet is brighter by ∼20 per cent, which should be relatively straightforward to detect in interferometric maps of regions around massive, young stars.

Key words: stars: formation – ISM: evolution – H II regions– ISM: kinematics and dynamics.

1 INTRODUCTION

A considerable amount of observational (see e.g. Reipurth et al. 1998; Bally & Reipurth 2003; Andrews et al. 2004; Smith, Bally & Walborn 2010; O'Dell et al. 2015) and theoretical (Raga et al. 2000; Masciadri & Raga 2001) work has been done on externally photoionized Herbig–Haro (HH) jets. These are typically outflows from low-mass stars, which are immersed in H II regions powered by massive stars (which are not the sources of the outflows).

A few known protostellar bipolar outflow systems appear to be ejected by massive young stars (see e.g. Poetzel, Mundt & Ray 1992; Alvarez & Hoare 2005). The best example of such a system is the HH 80/81 outflow (see e.g. the discovery paper of Reipurth & Graham 1988, and the recent paper of Masqué et al. 2015), which is ejected from a 1.7×10^4 $L_\odot$ source (Aspin & Geballe 1992). This source might reach the main sequence as a B star (Heathcote, Reipurth & Raga 1998).

Guzmán et al. (2012) made a multifrequency radio continuum systematic search of jets from high-mass stars with ATCA. From their detection rate, they estimated that the jet phase lasts 4×10^4 yr. Purser et al. (2016) have recently carried out a radio survey of ∼50 massive young stellar objects (YSOs), in which they identified 26 sources with jets and 14 with compact H II regions (see e.g. the review of Churchwell 2002). Also, Moscadelli et al. (2016) have started a survey of outflows from massive stars combining 22-GHz maser and radio continuum observations with high angular resolution. They find that 5 out of 11 sources clearly show a collimated outflow with very high momentum rates in the range of 10^{-3}–10^0 $M_\odot$ yr^{-1} km s^{-1}.

Furthermore, there is currently an intensive search for discs around massive stars (e.g. Cesaroni et al. 2017; for a recent review see Beltrán & de Wit 2016). The existence of these discs would indicate that massive stars form by disc accretion as a scaled-up version of low-mass stars. In this process, jets are a necessary ingredient to get rid of angular momentum and allow disc accretion. Thus, the detection of jets inside hypercompact (HC) and ultrahypercompact (UC) H II regions would also indicate that the accretion phase is active in this very early stage of young massive stars. In general, candidates to find these embedded jets are bipolar HCH II and UCH II like the prototype sources NGC 7538 IRS1 and MWC 349 A, which have been modelled as photoevaporated discs (e.g. Lugo, Lizano & Garay 2004). Other candidates are the HCH II regions G24.78+0.98 A1 (e.g. Beltrán et al. 2007), G11.92−061 MM1 (Ilee et al. 2016) and G023.01−00.41 (e.g. Sanna et al. 2016), which have associated bipolar outflows close to the plane of the sky, and the HCH II region G35.20−0.74N associated with an expanding precessing radio jet (Beltrán et al. 2016).

In this paper, we consider the situation in which a massive, young star (still embedded in the parental molecular cloud) that is powering a compact H II region is also ejecting a bipolar jet system. It is, of course, not completely clear if this situation actually occurs, and our paper is an attempt to predict the observational properties of such jets. These predictions will be useful for interpreting radio observations of massive YSOs.

This paper is organized as follows. In Section 2, we describe how a jet will trap a photoionization front close to the surface of

⋆ E-mail: raga@crya.unam.mx (ACR); l.rodriguez@crya.unam.mx (LFR); s.lizano@crya.unam.mx (SL)

the star, and will be neutral at larger distances. In Section 3, we derive a simple model for the H II region powered by the outflow source, and use it to compute the flux of diffuse, ionizing photons produced by the nebula. In Section 4, we derive a simple model for a conical, constant velocity jet that gets progressively ionized by the diffuse flux of the nebula that impinges on the walls of the cone. In Section 5, we choose possible physical parameters for the H II region/jet system, and estimate the values of the dimensionless parameters and characteristic distances that appear in our model. In Section 6, we compute a model for the chosen parameters, and make a prediction of the jet/surrounding H II region free–free intensity contrast. Finally, the implications of our results are discussed in Section 7.

2 THE EFFECT IN THE JET OF THE DIRECT, PHOTOIONIZING RADIATION FROM THE STAR

A massive young star is expected to have a very high mass-loss rate of $\sim 10^{-4}\,\mathrm{M}_{\odot}\,\mathrm{yr}^{-1}$ and a velocity of $\sim 1000\,\mathrm{km\,s}^{-1}$. If this jet is confined to a cone with an opening angle of a few degrees, the density at distances comparable to the stellar radius will be very high.

For example, for the above mass-loss rate and jet velocity, and for a stellar radius $R_* = 10\,\mathrm{R}_{\odot}$ (as appropriate for an O7 main-sequence star) and a half-opening angle $\alpha = 5^{\circ}$ (for the jet cone), assuming a constant velocity jet one obtains a number density $n \approx 5 \times 10^{12}\,\mathrm{cm}^{-3}$ close to the star. Because of this high density, the jet cone will trap an ionization front (IF) at distances comparable to the stellar radius, and will be neutral at larger distances from the star.

A realistic model of this region would require a description of the flow close to the stellar surface (including the jet acceleration region, which probably has strong departures from a radial flow). However, it is unavoidable that this region will have densities of the order of magnitude estimated above, and that the ionizing radiation from the star will be trapped by the jet at distances comparable to the stellar radius.

Therefore, at larger distances from the source, the jet from a massive, young star will be neutral. This neutral beam will then be bathed by the diffuse, ionizing radiation of the compact H II region that surrounds the star (which is produced as a result of the action of the stellar ionizing radiation on the surrounding interstellar medium). This radiation is described in the following section.

3 THE DIFFUSE, IONIZING RADIATION

As concluded in Section 2, a conical jet ejected from a young, massive star traps the stellar ionizing radiation, and at a distance $\sim R_*$, it becomes neutral. The outer walls of the neutral cone will then be photoionized by the diffuse ionizing radiation emitted by the associated, compact H II region.

For the case of a conical shape with a small opening angle, the radiation flux coming through the outer surface of the cone is approximately equal to the radiation flux through a surface parallel to the axial direction (which points away from the central source). This flux can be estimated as follows.

We first construct a simple model for a homogeneous, dust-free ionization-bounded nebula. To this effect, we consider a homogeneous gas sphere with almost fully ionized H, extending out to the Strömgren radius R_{S}, as shown in the schematic diagram of Fig. 1.

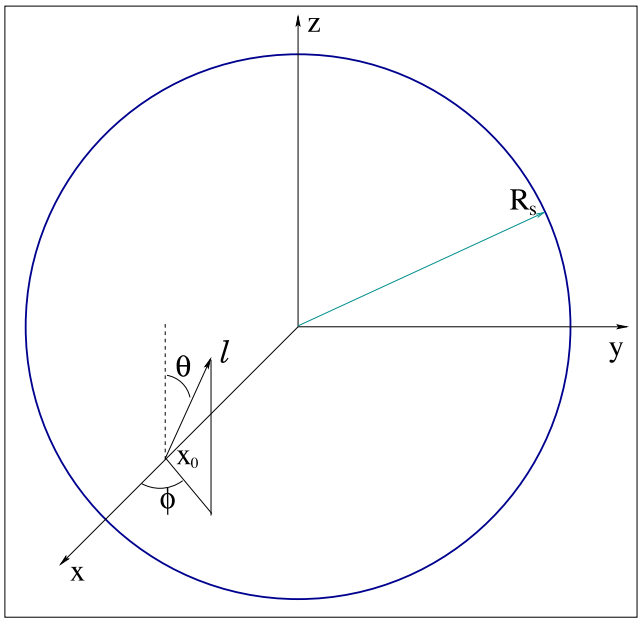

Figure 1. Schematic diagram of a Strömgren sphere of radius R_{S}. We consider a point (x_0, 0, 0) along the x-axis. We then solve the radiative transfer equation (for ionizing radiation) along lines of sight that go through this point. The angles θ and ϕ specify the direction and l is the distance along the line of sight.

The flux of 'direct' (i.e. emitted by the central star) ionizing photons at a distance R can be obtained from the relation

$$S_* = 4\pi R^2 F + \frac{4\pi}{3} R^3 n_{\mathrm{H}}^2 \alpha_{\mathrm{H}}, \tag{1}$$

where S_* is the stellar ionizing photon rate, n_{H} is the (homogeneous) H number density, α_{H} is the case B recombination coefficient (evaluated at a temperature $\approx 10^4$ K) and F is the number of ionizing photons per unit time and area going through a sphere of radius R. The second term on the right-hand side of equation (1) is the total number of recombinations per unit time inside the region of radius R. From this equation, we can obtain the flux as a function of radius:

$$F = \left[1 - \left(\frac{R}{R_{\mathrm{S}}}\right)^3\right] \left(\frac{R_{\mathrm{S}}}{R}\right)^2 \frac{S_*}{4\pi R_{\mathrm{S}}^2}, \tag{2}$$

where

$$R_{\mathrm{S}} = \left(\frac{3 S_*}{4\pi n_{\mathrm{H}}^2 \alpha_{\mathrm{H}}}\right)^{1/3} \tag{3}$$

is the Strömgren radius of a homogeneous nebula. We note that equation (2) is the 'inner solution' of Strömgren (1939), which can be obtained combining the radiative transfer equation (for ionizing photons) and the photoionization equilibrium condition (also see Raga 2015).

Also, the standard solution to the radiative transfer from a point-like stellar source (see e.g. the book of Osterbrock 1989) is

$$F = \frac{S_*}{4\pi R^2} \mathrm{e}^{-\tau_R}, \tag{4}$$

where τ_R is the radial optical depth given by

$$\tau_{\mathrm{R}} = n_{\mathrm{H}} \sigma_{\mathrm{H}} \int_0^R (1 - X)\, \mathrm{d}R', \tag{5}$$

where $1 - X$ (assumed to be $\ll 1$ within the ionized nebula) is the fraction of neutral H and $\sigma_{\rm H}$ is the photoionization cross-section of H. $X = n_{\rm H\,II}/n_{\rm H}$ is the ionization fraction. For photoionization by a stellar continuum (which falls rapidly for frequencies above the Lyman limit), we have $\sigma_{\rm H} \approx 6.3 \times 10^{-18}\,{\rm cm}^2$, the value of the photoionization cross-section of H at the Lyman limit.

Comparing equations (2) and (4), we obtain

$$e^{-\tau_R} = 1 - \left(\frac{R}{R_{\rm S}}\right)^3, \tag{6}$$

and taking the logarithmic derivative of this equation, we obtain

$$\frac{d\tau_R}{dR} = \frac{1}{R_{\rm S}} \frac{3(R/R_{\rm S})^2}{1-(R/R_{\rm S})^3} = (1-X) n_{\rm H} \sigma_{\rm H}, \tag{7}$$

where the second equality is obtained by taking the radial derivative of equation (5).

We now compute the flux of diffuse, ionizing photons (produced by recombinations to the $n = 1$ level of H) passing through a surface parallel to the radial direction. This is done as follows.

The number of Lyman continuum photons emitted per unit volume and solid angle by the gas is

$$j_{\rm d} = \frac{n_{\rm H}^2 \alpha_1}{4\pi}, \tag{8}$$

where $n_{\rm H}$ is the (uniform) H number density and α_1 is the recombination coefficient to the ground state of H (calculated at the uniform nebular temperature of $\approx 10^4$ K).

We now calculate the intensity arriving at a point $(x_0, 0, 0)$ (given in terms of the components of the Cartesian coordinate system shown in Fig. 1) as

$$I(x_0, \theta, \phi) = \int_0^{l_{\rm S}} j_{\rm d} e^{-\tau}\, dl, \tag{9}$$

where θ and ϕ are the usual direction angles (defined in Fig. 1) and l is the distance measured along the (θ, ϕ)-direction. In equation (9), $l_{\rm S}$ is the distance along the (θ, ϕ)-direction from the $(x_0, 0, 0)$ point to the outer edge of the nebula. This distance is given by

$$\frac{l_{\rm S}(x_0, \theta, \phi)}{R_{\rm S}} = -\left(\frac{x_0}{R_{\rm S}}\right) \cos\phi \sin\theta + \sqrt{\left(\frac{x_0}{R_{\rm S}}\right)^2 (\cos^2\phi \sin^2\theta - 1) + 1}. \tag{10}$$

The optical depth τ along the l-direction is

$$\tau = \int_0^l n_{\rm H}(1-x)\sigma_{\rm H} dl', \tag{11}$$

where the integrand is given by the second and third terms of equation (7), computed at a radius

$$R = \sqrt{x_0^2 + 2 x_0 l \cos\phi \sin\theta + l^2}. \tag{12}$$

We can now calculate the diffuse flux through a surface parallel to the radial direction as

$$F_{\rm d}(R) = 2 \int_0^{\pi} \int_0^{\pi/2} I(R, \theta, \phi)\, \cos\theta \sin\theta\, \, d\theta\, d\phi. \tag{13}$$

This double integral can be straightforwardly evaluated numerically to obtain the diffuse flux as a function of radius, the result of which is shown in Fig. 2. We note that the resulting radial dependence can be fitted by an analytic function of the form

$$\frac{F_{\rm d}(R/R_{\rm S})}{n_{\rm H}^2 \alpha_1 R_{\rm S}} = 0.187\, f_{\rm d}(R/R_{\rm S}), \tag{14}$$

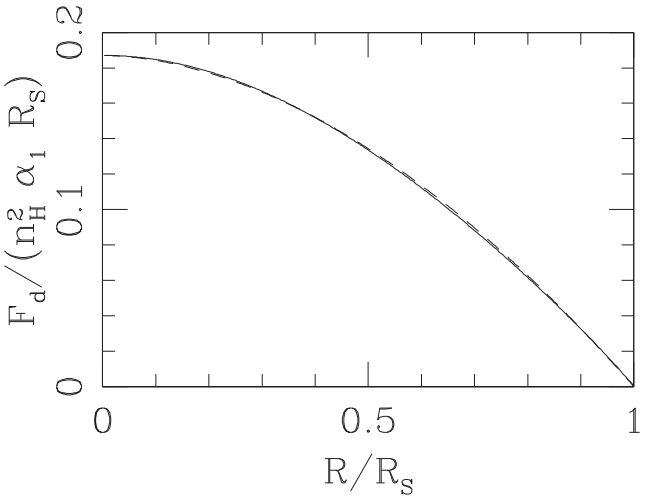

Figure 2. Flux $F_{\rm d}$ of the diffuse, ionizing radiation through a surface parallel to the radial direction, given as a function of distance R from the source. The solid curve is the numerical solution of equation (13), and the dashed curve is the analytic fit given by equations (14)–(15).

with

$$f_{\rm d}(R/R_{\rm S}) = 1 - (R/R_{\rm S})^{1.83}. \tag{15}$$

This analytic fit is also shown in Fig. 2.

This calculation is done with a simple H II region model in which we have assumed that the neutral fraction satisfies the condition $1 - x \ll 1$. This is the condition under which Strömgren (1939) derived his 'inner solution', and is not valid in the region close to the Strömgren radius $R_{\rm S}$, where we have the transition from ionized to neutral gas at the outer edge of the ionization-bounded nebula. This region, however, is very thin for the case of a stellar ionizing source, and not having a correct description of this region does not have an appreciable effect on the calculation of the diffuse ionizing flux.

We should note that Williams & Henney (2009) have computed similar H II region models in order to evaluate the importance of the diffuse, ionizing photon flux. However, they show only results for the diffuse flux through surfaces perpendicular to the radial direction (they actually have a qualitative discussion of the fluxes through surfaces parallel to the radial direction, but do not show graphs of these fluxes). These authors also studied other configurations, with radially dependent nebular densities and with different values of $\sigma_{\rm H}$ for the direct radiation from the source (appropriate for sources with 'hard' extreme-ultraviolet photon distributions).

4 SIDEWAYS PHOTOIONIZATION BY THE DIFFUSE FIELD

We now consider an initially neutral, conical jet flow from a massive star, with a small half-opening angle α, constant velocity $v_{\rm j}$ and mass-loss rate $\dot{M}_{\rm j}$. This conical jet travels within a surrounding H II region (produced by the same stellar source), and the outer walls of the cone therefore receive the diffuse, ionizing flux calculated in Section 3.

Fig. 3 shows a schematic diagram of the flow. The cylindrically symmetric jet (shown in an x, r cylindrical reference system) has an outer radius $r_{\rm j}$. The IF driven into the jet beam has a locus $r_{\rm i}(x)$.

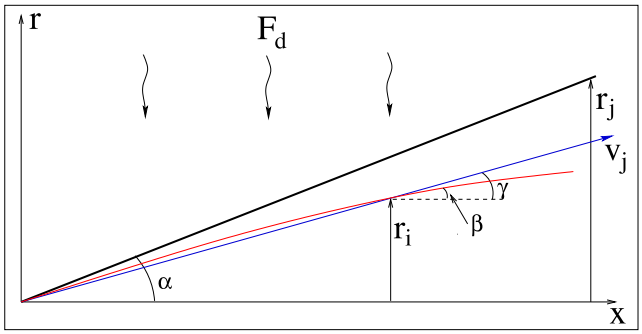

Figure 3. Schematic diagram of an initially neutral, conical jet from a young, massive star that is being photoionized by the diffuse field of the surrounding H II region. In a cylindrical (x, r) coordinate system, the jet cone (of half-opening angle α) is the solid, thick straight line $r_j(x)$. The jet velocity v_j points radially away from the origin (blue line). The diffuse, ionizing flux F_d drives an IF into the jet, which has a locus $r_i(x)$. The angle between the local direction of the flow and the x-axis is γ. The angle between the IF (red curve) and the x-axis is β.

The angles β (between the IF and the x-axis) and γ (between the jet velocity and the x-axis) obey the relations

$$\tan\beta = \frac{\mathrm{d}r_i}{\mathrm{d}x} \approx \beta, \qquad \tan\gamma = \frac{r_i}{x} \approx \gamma, \tag{16}$$

where the second equalities are valid for the small-angle regime.

The flux of neutral jet material that comes through the IF is

$$F_N = n_j v_j \sin(\gamma - \beta) \approx n_j v_j \left(\frac{r_i}{x} - \frac{\mathrm{d}r_i}{\mathrm{d}x} \right), \tag{17}$$

where the second equality is obtained using equation (16) and the small-angle approximation.

The number of recombinations in the outer, photoionized layer of the jet per unit area and time is

$$\dot{N}_{rec} = (r_j - r_i) n_j^2 \alpha_H, \tag{18}$$

where n_j is the (position-dependent) jet density and α_H is the case B recombination coefficient of H (in our simple analytic model, we assume that H and He have the same photoionization and recombination rates, so that we do not treat them independently). As the photoionized outer layer of the jet will have a temperature of $\sim 10^4$ K, we can assume that α_H does not depend on position.

For a constant-velocity, conical jet, the density as a function of spherical radius is given by

$$n_j = \frac{\dot{m}_j}{R^2 v_j} \approx \frac{\dot{m}_j}{x^2 v_j}, \tag{19}$$

with

$$\dot{m}_j = \frac{\dot{M}_j}{2\pi(1-\cos\alpha)\bar{m}} \approx \frac{\dot{M}_j}{\pi\alpha^2 \bar{m}}, \tag{20}$$

where $\bar{m} = 1.3 m_H$ for a gas with 90 per cent H and 10 per cent He (by number). The second equalities in equations (19)–(20) correspond to the small-angle limit.

Using the small-angle versions of equations (17)–(20), the balance equation

$$F_d = F_N + \dot{N}_{rec} \tag{21}$$

(where F_d is the sideways flux of diffuse, ionizing photons) is a differential equation involving the $\mathrm{d}r_i/\mathrm{d}x$ derivative (see equation 17). After some simple algebra, one obtains the dimensionless differential equation

$$\frac{\mathrm{d}q}{\mathrm{d}\xi} = q\frac{\xi - 1}{\xi^2} + \kappa\xi^2, \tag{22}$$

where

$$\begin{aligned} q &= \frac{r_j - r_i}{L_j} = \alpha\xi - \eta, \\ \eta &= r_i/L_j, \\ \xi &= x/L_j, \\ L_j &= \frac{\dot{m}_j \alpha_H}{v_j^2}, \\ \kappa &= \frac{F_d \dot{m}_j \alpha_H^2}{v_j^4}, \end{aligned} \tag{23}$$

where the diffuse flux F_d is given by equations (14)–(15) for the case of a homogeneous surrounding H II region.

As can be seen from Fig. 2, if the region in which the conical jet is being photoionized (by the diffuse radiation field) extends to distances $<0.3R_S$ (where R_S is the Strömgren region of the H II region, see equation 3), κ is approximately constant (as a function of distance x or $\xi = x/L_j$ from the source), and equation (22) then has the solution

$$q(\xi) = \frac{\kappa\xi}{2}\left[\xi(\xi-1) + \mathrm{e}^{1/\xi}\, E_1\left(\frac{1}{\xi}\right)\right], \tag{24}$$

where E_1 is the exponential integral. The locus $r_i(\xi)$ of the IF can then be calculated using equation (23).

Using equations (23) and (24), we then obtain the dimensionless radius $\eta = r_i/L_j$ of the IF as a function of dimensionless distance ξ:

$$\eta = \xi\left\{\alpha - \frac{\kappa}{2}\left[\xi(\xi-1) + \mathrm{e}^{1/\xi} E_1\left(\frac{1}{\xi}\right)\right]\right\}. \tag{25}$$

In Fig. 4, we show this solution for $\kappa = 0.1, \ldots, 10^4$ (in a factor of 10 steps), and an $\alpha = 0.1$ (radians) half-opening angle for the jet cone. This figure shows the outer radius of the jet r_j/L_j (dotted lines) and the radius of the IF $\eta = r_i/L_j$ (solid lines) as a function of dimensionless distance $\xi = x/L_j$ (see equation 23) from the source.

It is clear that for all κ values the diffuse ionizing field succeeds in photoionizing all of the conical jet beam at sufficiently large distances from the outflow source. This full photoionization will, of course, only be realized if the Strömgren radius of the surrounding H II region is large enough: If not, the jet will exit the nebula with a photoionized envelope and a neutral core.

It is also possible to obtain the following 'large κ', approximate analytic solution. For large values of κ, there is an approximate balance between the two terms on the right-hand side of equation (22). Balancing these two terms, we obtain the approximate solution

$$q_a = \frac{\kappa\xi^4}{1-\xi} \approx \kappa\xi^4, \tag{26}$$

where for the second equality, we have used the fact that for large κ values the neutral jet core extends only to distances $\xi \ll 1$ from the source (see Fig. 4). In this regime, the locus of the IF is then

$$\eta_a = \frac{r_i}{L_j} = \alpha\xi - \kappa\xi^4, \tag{27}$$

where we have used equations (23) and (26). These solutions are also shown in Fig. 4, in which we see that for $\kappa \geq 100$ the $\eta_a(\xi)$

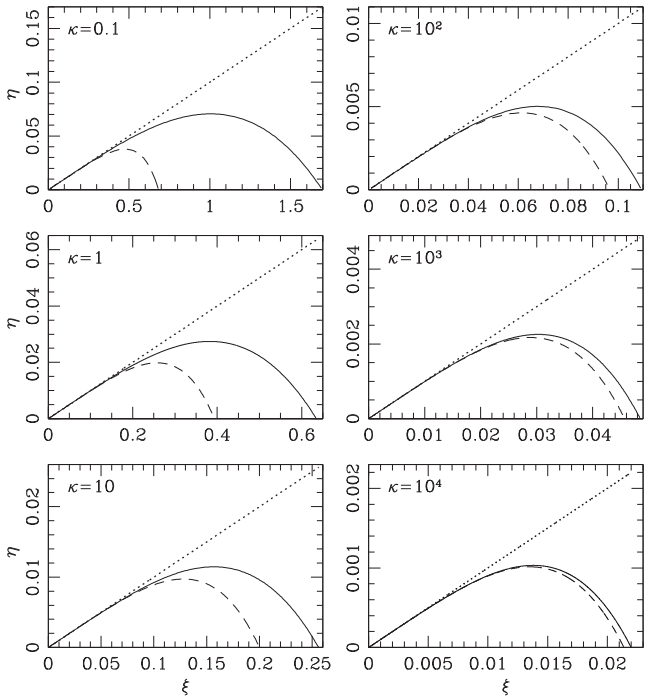

Figure 4. Constant κ solutions (i.e. with position-independent diffuse, ionizing flux F_d, see equation 23). The six frames show solutions with $\alpha = 0.1$ and $\kappa = 0.1$ (top left-hand panel) up to $\kappa = 10^4$ (bottom right-hand panel), in a factor of 10 steps. In all frames, the dotted line is the $r_j(x)/L_j$ dimensionless outer boundary of the jet. The solid line is the $\eta = r_i/L_j$ locus of the IF given by equation (25) and the dashed lines are the approximate solutions given by equation (27). The abscissa is the dimensionless axial coordinate $\xi = x/L_j$ (see equation 23).

solutions agree well with the results obtained from the full analytic solution (equation 24).

Finally, from equation (27) we can calculate the distance from the outflow source

$$\xi_m = \frac{x_m}{L_j} = \left(\frac{\alpha}{\kappa}\right)^{1/3} \tag{28}$$

at which the conical jet beam becomes fully ionized.

This 'high-κ' solution (equations 26–28) is, of course, also valid for the case of a variable κ, as would be found for the case of a jet with a neutral core extending over a substantial fraction of the Strömgren radius of the surrounding H II region (see equations 14–15 and 23). Such a solution is explored in Section 6.

5 THE VALUES OF THE PHYSICAL PARAMETERS

From Section 4, we see that in order to calculate a solution of the sideways photoionization of a conical jet, we have to specify the half-opening angle α and the dimensionless function κ (see equation 23). This function was assumed to be constant in the models shown in Fig. 4.

For the case of a homogeneous, surrounding H II region, we can use the definition of κ (see equation 23) and the diffuse, ionizing field of equations (14)–(15) to obtain

$$\kappa = \kappa_0 f_d(R/R_S), \tag{29}$$

where the function f_d is given by equation (15) and

$$\kappa_0 = 0.187 \frac{n_H^2 \alpha_1 R_S \dot{m}_j \alpha_H^2}{v_j^4}$$
$$= 2283 \left(\frac{S_*}{10^{49}\ \mathrm{s^{-1}}}\right)^{1/3} \left(\frac{n_H}{10^5\ \mathrm{cm^{-3}}}\right)^{4/3} \left(\frac{\dot{M}_j}{10^{-4}\ \mathrm{M_\odot\ yr^{-1}}}\right)$$
$$\times \left(\frac{1000\ \mathrm{km\ s^{-1}}}{v_j}\right)^4 \left(\frac{5^\circ}{\alpha}\right)^2. \tag{30}$$

For the second equality, we have assumed that the compact H II region has an $n_H = 10^5\ \mathrm{cm^{-3}}$ number density and that it is being photoionized by a source producing an $S_* = 10^{49}\ \mathrm{s^{-1}}$ ionizing photon rate. We have also assumed a temperature of 10^4 K for the ionized gas, therefore fixing the values of the recombination coefficients $\alpha_H = 2.55 \times 10^{-13}\ \mathrm{cm^3\ s^{-1}}$ (case B) and $\alpha_1 = 1.57 \times 10^{-13}\ \mathrm{cm^3\ s^{-1}}$ (to the ground state of H). For the jet, we have considered a half-opening angle $\alpha = 5^\circ$, a mass-loss rate $\dot{M}_j = 10^{-4}\ \mathrm{M_\odot\ yr^{-1}}$ and a velocity $v_j = 1000\ \mathrm{km\ s^{-1}}$.

With these parameters, we obtain the characteristic distance L_j (see equation 23)

$$L_j = 3.13 \times 10^{18}\ \mathrm{cm} \left(\frac{\dot{M}_j}{10^{-4}\ \mathrm{M_\odot\ yr^{-1}}}\right)$$
$$\times \left(\frac{1000\ \mathrm{km\ s^{-1}}}{v_j}\right)^2 \left(\frac{5^\circ}{\alpha}\right)^2, \tag{31}$$

and a Strömgren radius (see equation 3)

$$R_S = 9.78 \times 10^{16}\ \mathrm{cm} \left(\frac{S_*}{10^{49}\ \mathrm{s}}\right)^{1/3} \left(\frac{10^5\ \mathrm{cm^{-3}}}{n_H}\right)^{2/3}. \tag{32}$$

Combining equations (32)–(33), we then obtain

$$\frac{R_S}{L_j} = 0.0312 \left(\frac{S_*}{10^{49}\ \mathrm{s}}\right)^{1/3} \left(\frac{10^5\ \mathrm{cm^{-3}}}{n_H}\right)^{2/3}$$
$$\times \left(\frac{10^{-4}\ \mathrm{M_\odot\ yr^{-1}}}{\dot{M}_j}\right) \left(\frac{v_j}{1000\ \mathrm{km\ s^{-1}}}\right)^2 \left(\frac{\alpha}{5^\circ}\right)^2. \tag{33}$$

Finally, for the chosen parameters, the position-dependent jet density (see equation 19) is given by

$$n_j = 125.8\ \mathrm{cm^{-3}} \left(\frac{\alpha}{5^\circ}\right)^2 \left(\frac{10^{-4}\ \mathrm{M_\odot\ yr^{-1}}}{\dot{M}_j}\right)$$
$$\times \left(\frac{v_j}{1000\ \mathrm{km\ s^{-1}}}\right)^3 \frac{1}{\xi^2}. \tag{34}$$

From equation (30), we see that for the H II region + outflow parameters chosen in this section, we expect

(i) a large value of κ_0 between 10^3 and 10^4;
(ii) a jet characteristic length $L_j \sim 10^{18}$ cm;
(iii) a Strömgren radius (for the nebula) $R_S \sim 0.03 L_j$.

Interestingly, the 'constant $\kappa = 10^3$ and 10^4' models of Fig. 4 (see also Section 4) show that the neutral core of the conical jet extends out to a distance of ∼0.02–0.05 L_j, basically out to the Strömgren radius of the nebula.

Of course, a more precise evaluation of whether or not the jet becomes fully ionized by the diffuse radiation of the H II region requires calculating models with a variable κ (see equation 29), as the diffuse flux drops on approaching the Strömgren radius (see Fig. 2). This is done in the next section of this paper.

6 A JET WITHIN A COMPACT H II REGION

Let us now consider a conical jet photoionized by a diffuse field with a radial dependence resulting in

$$\kappa = \kappa_0 \left[1 - (R/R_S)^\beta\right], \tag{35}$$

where $\beta = 1.83$ for the case of a jet embedded in a uniform H II region (see equation 15).

For this functional form of κ, equation (22) can be integrated (setting $R = L_0\xi$ in equation 35) to obtain

$$q = \frac{\kappa_0\xi}{2}\left[\xi(\xi-1) + \mathrm{e}^{1/\xi}E_1\left(\frac{1}{\xi}\right) + 2\left(\frac{L_j}{R_S}\right)^\beta \mathrm{e}^{1/\xi}\Gamma(-\beta-2, 1/\xi)\right], \tag{36}$$

where E_1 is the exponential integral and Γ is the upper incomplete gamma function.

We now take the H II region ($n_H = 10^5\,\mathrm{cm}^{-3}$, $S_* = 10^{49}\,\mathrm{s}^{-1}$ and $T = 10^4$ K) and jet parameters ($\alpha = 5^\circ$, $\dot{M}_j = 10^{-4}\,\mathrm{M}_\odot\,\mathrm{yr}^{-1}$ and $v_j = 1000\,\mathrm{km\,s}^{-1}$) of the previous section. These parameters result in $\kappa_0 = 2300$, $L_j = 3.13 \times 10^{18}$ cm and $R_S = 9.78 \times 10^{16}$ cm (see equations 30–32).

With these parameters, we can either integrate numerically equation (22) or evaluate the special functions in the analytic solution (given by equation 36 with $\beta = 1.83$). From the resulting $q(R)$, we compute the radius $r_i(R)$ of the neutral core (see equation 23), which we show on the top frame of Fig. 5. In this frame, we also show the corresponding, high-κ analytic solution (see equation 27).

In Fig. 5, we see that for distances from the source out to $x \sim 6 \times 10^{16}$ cm, the locus $r_i(x)$ of the IF follows a curve similar to the ones of the 'constant-κ' solutions (see Fig. 4). For larger distances from the source, $r_i(x)$ starts increasing because of the drop of the diffuse ionizing flux F_d towards the edge of the H II region (see Section 3 and Fig. 2).

We now estimate the contrast between the free–free emission of the jet and the emission of the H II region. The intensity of the jet (averaged over the jet cross-section) above the emission of the surrounding nebula is

$$\Delta I = \frac{\pi\beta_{ff}}{2}\left(n_j^2\frac{r_j^2 - r_i^2}{r_j} - r_j n_H^2\right), \tag{37}$$

where we have subtracted the 'missing average emission' $\pi r_j^2 n_H^2 \beta_{ff}/(2r_j)$ of the region of the nebula occupied by the jet cone. In equation (37), $n_e n_H \beta_{ff}$ is the free–free emission coefficient (with β_{ff} evaluated at the local temperature, which we assume to be 10^4 K for both the jet and the H II region).

As the central free–free intensity of the H II region is $I_c = 2R_S n_H^2 \beta_{ff}$, the contrast between the jet intensity and the H II region is

$$\frac{\Delta I}{I_c} = \frac{\pi}{4R_S}\left[\left(\frac{n_j}{n_H}\right)^2\frac{r_j^2 - r_i^2}{r_j} - r_j\right], \tag{38}$$

where the position-dependent jet density n_j is given by equation (34). From equation (38), it is clear that $\Delta I/I_c$ can have both positive (i.e. the jet being brighter than the background H II region) or negative (the jet appearing darker than the H II region) values.

In Fig. 5, we show the resulting jet/central H II region free–free intensity contrast (equation 38) resulting from the numerical integration of equation (22) and from the approximate, high-κ analytic solution (see equations 26–27). From this plot, we see that close to the source the jet has an overbrightness (with respect to the surrounding H II region) of ≈18 per cent of the central H II region brightness. At radii larger than $\sim 8 \times 10^{16}$ cm, the jet cone has a negative intensity contrast (i.e. it shows up as a 'dark streak' against the background H II region).

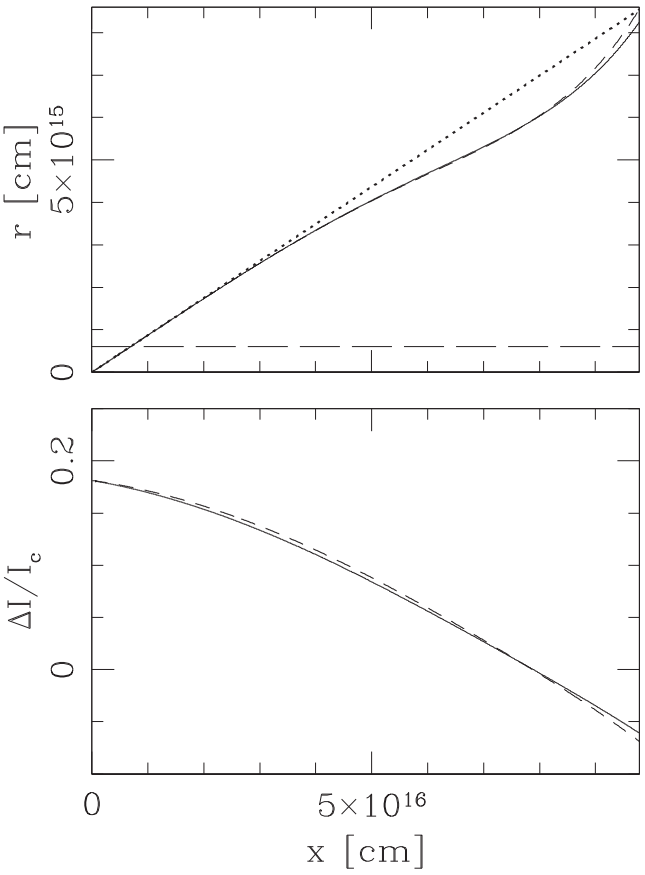

Figure 5. Solutions for the jet/H II region, 'variable-κ" model of Section 6. The top frame shows the jet cone (dotted line) and the locus of the IF (solid line → numerical integration of equation 22; short-dashed line → approximate solution of equation 27). The horizontal, long-dashed line (top frame) shows a 0.1 arcsec angular size at an assumed distance of 400 pc to the astrophysical object. The bottom frame shows the intensity of the jet (above the background H II region, see equation 38) calculated with a numerical solution of equation (22) or with equation (36) (solid line) and with the approximate solution of equation (26) (dashed line). The x-axis ends at the Strömgren radius.

In Fig. 5 (top frame), we also show the size of a 0.1 arcsec beam (assumed for an interferometric observation) for an object at a distance of 400 pc (e.g. in the Orion star formation region). We see that the jet beam would be resolved (and therefore its intensity not affected by 'beam smearing') at distances larger than $\sim 10^{16}$ cm from the outflow source.

7 CONCLUSIONS

We present a simple model of a young, massive star that photoionizes a compact H II region, and also ejects a conical jet. For parameters appropriate for a young, massive star, the conical jet will trap an IF at a distance close to the stellar radius, and will have a neutral beam at larger distances from the outflow source (see Section 2). The surface of this neutral, conical beam will then be partially photoionized by the diffuse, ionizing radiation produced by the surrounding H II region (Sections 3–6).

We develop a simple model that describes the penetration into the conical jet beam of an IF. We find a full analytic solution for the case in which the diffuse, ionizing radiation field is constant (i.e. without a radial dependence). We also find a simpler analytic solution that is also valid for the case of a radially dependent diffuse ionizing field (see Section 4).

We then present the analytical solution for a given choice of parameters for the star, H II region and jet (Section 5), and calculate the contrast between the free–free continuum emission of the jet (above the emission of the surrounding H II region) and the central intensity of the H II region. We find that the region of the jet close to the outflow source has an intensity ∼20 per cent higher than the H II region. This should be relatively easily detected in interferometric observations of compact H II regions.

This model has been computed for a jet surrounded by a uniform, dust-free H II region (see Sections 3 and 5). As many compact H II regions show a shell-like structure, the diffuse ionizing field impinging on the walls of the conical jet might be somewhat higher than the one of our model (see fig. 4 of Williams & Henney 2009), which would result in higher free–free intensities for the jet than the ones shown in Fig. 5. Another interesting effect is the possible presence of dust within the compact H II region (see e.g. Petrosian, Silk & Field 1972; Franco, Tenorio-Tagle & Bodenheimer 1990), which would reduce the size of the H II region and produce an internal density stratification (through the effect of radiation pressure on dust, see Draine 2011 ; Rodríguez-Ramírez et al. 2016).

The prediction of our model is that a jet from a massive, young star should stand out against the background, compact H II region by ∼20 per cent (in angularly resolved, interferometric maps). Such an intensity contrast should be detectable in high signal-to-noise ratio interferometric maps of compact H II regions.

Our present models have important approximations:

(i) It is implicitly assumed that we always have a fast 'R-type' IF, which does not produce a hydrodynamical perturbation of the jet flow. This, of course, will not be the case in situations where the front stops penetrating the jet beam (see e.g. the numerical simulations of Raga et al. 2000).

(ii) The radiative transfer is calculated in a 'planar approximation'. This approximation is strictly valid for a thin ionized layer at the outer boundary of the jet cone, but will become progressively worse for describing the full ionization of the jet cone. Better approximations would be to use the cylindrical 'two-stream' approximation of Cantó et al. (1998), or to carry out numerical simulations with a full 'discrete ordinate' radiative transfer calculation.

(iii) In order to carry out the prediction of the free–free emission, we have assumed that both the jet and the surrounding H II region are optically thin. It is clear that depending on the densities of the object and the frequency at which the radio observation is carried out, this might not be an appropriate assumption.

If jet flows within compact H II regions are identified in the future, it will clearly become worthwhile to calculate more detailed models.

ACKNOWLEDGEMENTS

ACR acknowledges support from the CONACyT grants 167611 and 167625 and the DGAPA-UNAM grants IA103315, IA103115, IG100516 and IN109715. SL acknowledges support from the CONACyT 153522 and DGAPA-UNAM 105815 grants. We thank Sam Falle (the referee) for helpful comments.

REFERENCES

Alvarez C., Hoare M. G., 2005, A&A, 440, 569
Andrews S. M., Reipurth B., Bally J., Heathcote S. R., 2004, ApJ, 606, 353
Aspin C., Geballe T. R., 1992, A&A, 266, 219
Bally J., Reipurth B., 2003, AJ, 126, 893
Beltrán M. T., de Wit W. J., 2016, A&AR, 24, 6
Beltrán M. T., Cesaroni R., Moscadelli L., Codella C., 2007, A&A, 471, L13
Beltrán M. T., Cesaroni R., Moscadelli L., Sánchez-Monge Á., Hirota T., Kumar M. S. N., 2016, A&A, 593, A49
Cantó J., Raga A. C., Steffen W., Shapiro P. R., 1998, ApJ, 502, 695
Cesaroni R. et al., 2017, A&A, 602, A59
Churchwell E., 2002, ARA&A, 40, 27
Draine B. T., 2011, ApJ, 732, 100
Franco J., Tenorio-Tagle G., Bodenheimer P., 1990, ApJ, 349, 126
Guzmán A. E., Garay G., Brooks K. J., Voronkov M. A., 2012, ApJ, 753, 51
Heathcote S., Reipurth B., Raga A. C., 1998, AJ, 116, 1940
Ilee J. D. et al., 2016, MNRAS, 462, 4386
Lugo J., Lizano S., Garay G., 2004, ApJ, 614, 807
Masciadri E., Raga A. C., 2001, A&A, 376, 1073
Masqué J. M., Rodríguez L. F., Araudo A., Estalella R., Carrasco-González C., Anglada G., Girart J. M., Osorio M., 2015, ApJ, 814, 44
Moscadelli L. et al., 2016, A&A, 585, A71
O'Dell C. R., Ferland G. J., Henney W. J., Peimbert M., García-Díaz Ma. T., Rubin R. H., 2015, AJ, 150, 108
Osterbrock D., 1989, Astrophysics of Gaseous Nebulae and Active Galactic Nuclei. University Science Books, Mill Valley, CA
Petrosian V., Silk J., Field G. B., 1972, ApJ, 177, L69
Poetzel R., Mundt R., Ray T. P., 1992, A&A, 262, 229
Purser S. J. D. et al., 2016, MNRAS, 460, 1039
Raga A. C., 2015, Rev. Mex. Astron. Astrofis., 51, 61
Raga A. C. et al., 2000, MNRAS, 314, 681
Reipurth B., Graham J. A., 1988, A&A, 202, 219
Reipurth B., Bally J., Fesen R. A., Devine D., 1998, Nature, 396, 343
Rodríguez-Ramírez J. C., Raga A. C., Lora V., Cantó J., 2016, ApJ, 833, 256
Sanna A., Moscadelli L., Cesaroni R., Caratti o Garatti A., Goddi C., Carrasco-González C., 2016, A&A, 596, L2
Smith N., Bally J., Walborn N. R., 2010, MNRAS, 405, 1153
Strömgren B., 1939, ApJ, 89, 526
Williams R. J. R., Henney W. J., 2009, MNRAS, 400, 263

This paper has been typeset from a TEX/LATEX file prepared by the author.